

## Search for Higgs boson in final states with lepton, missing energy, and at least two jets using $b$ -jet identification in $9.7 \text{ fb}^{-1}$ of Tevatron data

The DØ Collaboration  
URL <http://www-d0.fnal.gov>  
(Dated: March 5, 2012)

We present a search for the Higgs boson in final states with a charged lepton (electron or muon), missing energy, and two or three jets using  $b$ -jet identification in data corresponding to  $9.7 \text{ fb}^{-1}$  of integrated luminosity collected with the DØ detector at the Fermilab Tevatron  $p\bar{p}$  collider. The search is primarily sensitive to  $WH \rightarrow \ell\nu b\bar{b}$  production, though contributions from  $gg, VV \rightarrow H \rightarrow WW \rightarrow \ell\nu jj$  and  $VH \rightarrow VWW \rightarrow \ell\nu jjjj$  production are considered (where  $V = W$  or  $Z$ ). We observe good agreement between data and expected background. For  $M_H = 115 \text{ GeV}$  ( $M_H = 130 \text{ GeV}$ ) we set a 95% C.L. upper limit on the production of a standard model Higgs boson of  $3.96 \times \sigma_{SM}$  ( $4.88 \times \sigma_{SM}$ ); where  $\sigma_{SM}$  is the standard model cross section, while we expect a set a limit of  $3.15 \times \sigma_{SM}$  ( $6.11 \times \sigma_{SM}$ ).

*Preliminary Results for the 2012 Moriond EW conference*

## I. INTRODUCTION

The only unobserved fundamental particle in the standard model (SM) is the Higgs boson, predicted as a consequence of describing spontaneous electroweak symmetry breaking using the Higgs mechanism. Its observation would confirm the hypothesis that the Higgs mechanism generates the masses of the weak gauge bosons and also provide an explanation for the finite masses of fermions via their Yukawa couplings to the Higgs field. The mass of the Higgs boson ( $M_H$ ) is free parameter in the SM, but the combination of results from direct searches at the CERN  $e^+e^-$  Collider (LEP) [1] and precision measurements of other electroweak parameters constrain  $M_H$  to  $114.4 < M_H < 186$  GeV at 95% C.L [2]. The  $M_H$  region 156–177 GeV is excluded at the 95% C.L. by the CDF and D0 combined analysis [3]. ATLAS and CMS at the Large Hadron Collider (LHC) have excluded  $M_H$  values 112.7–115.5 GeV, 131–237 GeV, and 251–468 GeV (ATLAS) [4] and 127–600 GeV (CMS) [5] at the 95% C.L. The remaining allowed mass range is being probed further at the Fermilab Tevatron Collider. This paper describes searches for the SM Higgs boson in events with a charged lepton (electron or muon), missing energy, and two or three jets in the final state.

The dominant process for Higgs boson production at the Tevatron is gluon fusion, but additional production mechanisms, including associated production of a Higgs boson and a  $W$  or a  $Z$  boson and direct production via vector boson fusion, occur at rates reduced by roughly an order of magnitude. At masses below  $M_H \approx 135$  GeV, the branching fraction of  $H \rightarrow b\bar{b}$  dominates, while  $H \rightarrow WW$  is the favored decay channel above 135 GeV. In the low mass region, where the  $H \rightarrow b\bar{b}$  decay is favored, associated production of a Higgs boson and a  $W$  boson is among the most sensitive search channels at the Tevatron. Maximizing the sensitivity of the SM Higgs boson search also requires all channels to be exploited and combined. Studying final states with a lepton, missing energy, and two or three jets in the final state is primarily sensitive to  $WH \rightarrow \ell\nu b\bar{b}$  production. However, this final state also includes contributions from  $gg, VV \rightarrow H \rightarrow WV \rightarrow \ell\nu jj$  and  $VH \rightarrow VWW \rightarrow \ell\nu jjjj$  ( $V = W$  or  $Z$ ). The analysis is optimized for these varying production and decay mechanisms by organizing events into subchannels based on jet multiplicity and the number and quality of candidate  $b$ -quark jets. This strategy allows enhanced sensitivity in the intermediate  $M_H$  region near 135 GeV, where no single Higgs boson production and decay mechanism drives the combined search sensitivity.

Several searches for  $WH \rightarrow \ell\nu b\bar{b}$  production have already been published at a  $p\bar{p}$  center-of-mass energy of  $\sqrt{s} = 1.96$  TeV. Four of these [6–9] use subsamples ( $0.17 \text{ fb}^{-1}$ ,  $0.44 \text{ fb}^{-1}$ ,  $1.1 \text{ fb}^{-1}$  and  $5.3 \text{ fb}^{-1}$ ) of the data analyzed in this paper. A previous search in the  $H \rightarrow WW \rightarrow \ell\nu jj$  channel at D0 uses a  $5.4 \text{ fb}^{-1}$  subsample of the data used in this paper [10].

We present an updated search using a multivariate approach in  $9.7 \text{ fb}^{-1}$  of integrated luminosity collected by the D0 experiment. The search is based on events with one charged lepton ( $\ell = e$  or  $\mu$ ), an imbalance in transverse energy ( $\cancel{E}_T$ ) that arises from the neutrino in the  $W \rightarrow \ell\nu$  decay, and two or three jets, with one or two of these jets selected as candidate  $b$ -quark jets ( $b$ -tagged).

The channels are separated into orthogonal selections of events with two tight  $b$ -tagged jets, two loose  $b$ -tagged jets where at least one of them is not tight  $b$ -tagged jet, and one tight  $b$ -tagged jet, where there is no second loose  $b$ -tagged jet. Events that do not fall into one of these  $b$ -tag categories are not considered in this analysis. Single- $b$ -tagged events contain three important sources of backgrounds: (i)  $W$  boson production in association with light-quark jets and possibly one  $c$ -quark jet, (ii)  $W$  boson production in association with two heavy-flavor ( $b\bar{b}, c\bar{c}$ ) jets, and (iii) multijet events, where a jet is misidentified as an isolated lepton. In events with two tight  $b$ -tagged jets, the dominant backgrounds are from  $Wb\bar{b}$  and  $t\bar{t}$ . We use a Boosted Decision Tree (BDT) multivariate analysis technique to separate the SM background from signal in the selected events and search for an excess of data, expected primarily at large values of the BDT discriminant. A separate BDT discriminant is created for each combination of final state jet multiplicity (2 or 3), lepton flavor ( $e$  or  $\mu$ ), and  $b$ -tagged jet category. Because of detector upgrades and algorithm improvements, we split our data into four epochs: Run IIa (2002 – March 2006), Run IIb1 (June 2006 – August 2007), Run IIb2 (October 2007 – June 2009) and RunIIb34 (September 2009 – 2011). In total, we have 48 orthogonal subchannels. We consider all channels simultaneously when performing the search and the final limit setting.

This analysis uses most major components of the D0 detector [11]. The central-tracking system consists of a silicon microstrip tracker (SMT) and a central fiber tracker (CFT) located within a 2 T superconducting solenoidal magnet. The liquid-argon sampling calorimeter consists of a central section (CC), covering pseudorapidity  $|\eta| < 1.1$  relative to the center of the detector [12] and two end calorimeters (EC) extending coverage to  $|\eta| < 4.2$ . These three calorimeters are housed in separate cryostats [13], with scintillators between the CC and EC cryostats providing additional sampling of developing showers at  $1.1 < |\eta| < 1.4$ . The muon system is located beyond the calorimetry and consists of layers of tracking detectors and scintillation trigger counters before and after 1.8 T iron toroidal magnets. A 2006 detector upgrade added an additional layer of silicon to the SMT [14], an improved calorimeter trigger [15], and improved tracking electronics.

The luminosity is measured using plastic scintillator arrays located in front of the EC cryostats at  $2.7 < |\eta| < 4.4$ . We reject data in which the tracking, calorimeter, or muon information may have been compromised. The trigger

and data acquisition systems are designed to accommodate the high instantaneous luminosities ( $> 4 \times 10^{32} \text{ cm}^{-2}\text{s}^{-1}$ ) of Run II.

Events in the electron channel are triggered by a logical OR of several triggers requiring an electromagnetic (EM) object and one jet. Trigger efficiencies are taken into account in the simulation through a reweighting of events, based on an efficiency derived from data, and parametrized as a function of electron  $\eta$ , azimuth  $\phi$ , and jet  $p_T$ .

We accept events containing a muon from an inclusive mixture of single muon, muon plus jet,  $\cancel{E}_T$  plus jet, and multijet triggers. The MC events are first reweighted to correct the efficiency for events to be triggered by a subset of single muon and muon plus jet triggers. The additional efficiency of the complementary set of triggers is modeled as a function of the scalar sum of jet  $p_T$  ( $H_T$ ), muon  $\eta$  and muon  $\phi$ . We add the two efficiency corrections together to form the full (inclusive) data sample, providing approximately a 30% increase in efficiency over only using the single muon and muon plus jet triggers, and we observe good agreement between data and MC when combining the single muon and complementary triggers to form the inclusive dataset.

## II. SIMULATED DATASETS

Simulation of background and signal processes relies on the CTEQ6L1 [16, 17] leading-order parton distribution functions for all MC event generators. The  $W(Z)$ +jets and  $t\bar{t}$  events are generated with ALPGEN [18] interfaced to PYTHIA [19] for parton showering and hadronization. ALPGEN samples are produced using the MLM parton-jet matching prescription [18]. The  $W(Z)$ +jets samples contain  $W(Z)jj$  and  $W(Z)cj$  processes, while  $W(Z)b\bar{b}$  and  $W(Z)c\bar{c}$  are generated separately. The PYTHIA [19] MC generator is used to simulate the production of dibosons with inclusive decays ( $WW$ ,  $WZ$  and  $ZZ$ ), and all signal processes. Single top-quark events are generated with SingleTop event generator [20, 21] and use PYTHIA for parton evolution and hadronization. All generated events are processed through a full D0 detector simulation (based on GEANT [22]), using the same reconstruction software as used for D0 data. Data events from random beam crossings are overlaid to account for multiple  $p\bar{p}$  interactions.

The simulated background cross sections are normalized to the SM predictions, except for  $W/Z$ +jets events, which are normalized to data before applying  $b$ -tagging, where the contamination from signal is predicted to be negligible. The predicted signal cross sections are from Ref. [23]. NLO cross sections are used for  $t\bar{t}$  (resummed NLO) [24], single-top [25], and diboson [26, 27]. As a cross check, we compare data with the ALPGEN prediction for  $W$ +jets, corrected in such a way that the inclusive  $W$  production cross section is equal to its NNLO calculation [28] with MRST2004 NNLO PDFs [29], and we find a relative data/MC normalization factor of  $1.0 \pm 0.1$  for  $W$ +jets, where the normalization factor from data is obtained after subtracting all other expected background processes. For the  $W$ +heavy-flavor jet events, the phenomenological ratio of the ALPGEN prediction to NLO corrections for  $Wb\bar{b}$ ,  $Wc\bar{c}$ , and  $W$ +light jets (obtained from MCFM [27, 30]) is consistent with experiment, so that we do not apply additional corrections beyond those from MCFM.

## III. EVENT SELECTION

This analysis is based on the selection of events with exactly one electron with  $p_T > 15$  GeV and  $|\eta| < 1.1$  or  $1.5 < |\eta| < 2.5$ , or exactly one muon with  $p_T > 15$  GeV and  $|\eta| < 1.6$ . Events are also required to have  $\cancel{E}_T > 15$  (20) GeV for the electron (muon) channel, and exactly two or three jets with  $p_T > 20$  GeV (after calibration of the jet energy [31]) and  $|\eta| < 2.5$ .  $\cancel{E}_T$  is calculated from the individual calorimeter cells, ignoring unclustered energy in cells of the outermost readout layers of the calorimeter, and is corrected for the presence of any muons. All energy corrections to electrons or to jets are propagated into  $\cancel{E}_T$ .

Events with additional charged leptons, isolated from jets, that pass a flavor-dependent  $p_T$  threshold ( $p_T^e > 20$  GeV,  $p_T^\mu > 15$  GeV and  $p_T^\tau > 10$  or 15 GeV for hadronically decaying  $\tau$  lepton;  $\tau$  lepton identification is described in [32]) are rejected to suppress dilepton backgrounds from  $Z$ ,  $t\bar{t}$ , and  $WW$  events. Only events with a primary vertex (with at least three tracks) located within  $\pm 60$  cm of the nominal longitudinal interaction point, measured along the proton beam axis, are selected for further analysis.

Lepton candidates are identified in two steps: (i) Each candidate must pass “loose” identification criteria. For electrons, we require a loose cut on a multivariate discriminator that makes use of inputs that include: calorimeter energy over track momentum; fraction of total energy in a shower that is deposited in the EM section of the calorimeter; calorimeter isolation fraction (ratio of the EM energy in a  $\Delta\mathcal{R} < 0.2$  cone in the  $(\eta, \phi)$  space [12] to the total calorimeter energy in a  $\Delta\mathcal{R} < 0.4$  cone around the electron); calorimeter shower shape information; track match probability; track isolation information; track hits in SMT and CFT; tracker activity in projected electron road; central preshower hit information. For a loose muon, we require the timing of scintillator hits to coincide with beam crossings (to veto cosmic-rays), a match of the reconstructed track in the muon system with one in the central tracker, and isolation

from jets to reject muons from semileptonic decay of hadrons ( $\Delta\mathcal{R} > 0.5$ ). (ii) The loose leptons then undergo a final “tight” selection. Tight electrons must satisfy a more restrictive cut on the multivariate electron identifier. Tight muons must satisfy stricter isolation criteria on energy in the calorimeter and momenta of tracks near the trajectory of the muon candidate. Inefficiencies introduced by lepton-identification and isolation criteria are determined from  $Z \rightarrow \ell\ell$  data and used to correct the efficiency in simulated events to match that in the data. The final selections rely only on tight leptons, with loose leptons used to determine the multijet background.

#### IV. INSTRUMENTAL AND MULTIJET BACKGROUND MODELING

Instrumental backgrounds and those from semi-leptonic decays of hadrons, referred to jointly as the multijet background, are estimated from data. The instrumental background is important for the electron channel, where a jet with high EM fraction can pass electron-identification criteria, or a photon can be misidentified as an electron. In the muon channel, the multijet background is less significant, and arises mainly from the semi-leptonic decay of heavy quarks, where the muon satisfies the isolation requirements.

The multijet background is estimated in each channel based on events in data that pass the loose but fail the tight lepton identification criteria (i.e. “loose-not-tight” events). We first determine the probability,  $f_{T|L}$ , for a loose-lepton candidate originating from a jet to also pass tight identification. This is done in events that pass preselection requirements, i.e., they contain one loose lepton and two jets, but with small  $\cancel{E}_T$  (between 5 and 15 GeV). The total non-multijet background present with these selections is estimated from MC and subtracted from the data before estimating the contribution from multijet events. The probability  $f_{T|L}$  is defined by the ratio of the estimated multijet contribution including only tight leptons to that containing loose and tight leptons. For electrons,  $f_{T|L}$  is determined as a function of electron  $p_T$  in three regions of  $|\eta|$  and four in  $\Delta\phi(\cancel{E}_T, e)$ . For muons, it is determined as a weighted average of the  $f_{T|L}$  from individual functions in  $\Delta\phi(\cancel{E}_T, \mu)$ , second-leading jet  $p_T$ ,  $\cancel{E}_T$  and  $W$  transverse mass. Each loose-not-tight event is assigned a weight that contributes to the multijet estimation based on  $f_{T|L}$  as a function of event kinematics. Since  $f_{T|L}$  depends on  $\cancel{E}_T$ , the scale of this estimate of the multijet background must be adjusted when comparing to data with  $\cancel{E}_T > 15$  (20) GeV for electron (muon) channels. Before applying  $b$ -tagging, we perform a fit to the transverse mass of the  $W$  candidate ( $M_W^T$ ) distribution in the electron channel or a simultaneous fit to the muon  $p_T$  and  $\cancel{E}_T$  distributions to set the scale of the multijet and  $W/Z$ +jets backgrounds simultaneously. To suppress multijet background, events with  $M_W^T < 40 \text{ GeV} - 0.5 \cancel{E}_T \text{ GeV}$  are removed in both the electron and muon channels.

#### V. JET MODELING CORRECTIONS

Jets are reconstructed using a midpoint cone algorithm [33] with a radius of  $\Delta\mathcal{R} = \sqrt{(\Delta y)^2 + (\Delta\phi)^2} = 0.5$ , where  $y$  is the jet rapidity. Identification requirements ensure that the distribution in jet energy for all layers of the calorimeter is reasonable and that jets are not caused by noise or spurious depositions of energy. The difference in efficiency for jet identification and jet resolution between data and simulation is taken into account in the overall MC correction for jet reconstruction efficiency and energy resolution. Comparison of ALPGEN with other generators [34] and with data shows discrepancies in distributions of jet pseudorapidity and dijet angular separations. The data are therefore used to correct the ALPGEN  $W$ +jets and  $Z$ +jets MC events by reweighting the simulated  $\Delta\eta(\ell, j)$  distribution for both the leading and second-leading jets, the  $\Delta\mathcal{R}$  distribution between the two leading jets, and  $W$  boson  $p_T$  in the  $W/Z$ +jets samples through the use of polynomial functions that bring the total simulated background into agreement with the high statistics pre- $b$ -tagged data. After this step, the jet distributions in simulations are in agreement with the data over the complete range of kinematics.

#### VI. RESULTS

Efficient identification of  $b$ -jets is central to the search for  $WH$  production. The D0  $b$ -tagging algorithm for identifying heavy-flavored jets is based on a combination of variables sensitive to the presence of tracks or secondary vertices displaced significantly from the primary vertex. This algorithm makes use of the BDT and provides improved performance over the previous Neural Network based algorithm that is described in Ref. [35]. The efficiency is determined for taggable jets, where taggable jets have at least two tracks of good quality with at least one hit in the SMT. Simulated events are corrected to have the same fraction of jets satisfying the taggability and  $b$ -tagging requirements as found in preselected data. For jets that are not taggable, the  $b$ -tagging algorithm output is zero.

Cuts on the continuous  $b$ -ID discriminant output are used to define the tagging categories. Events with exactly one  $b$ -tagged jet are assigned to the one tight  $b$ -tag category, if the  $b$ -ID discriminant output is high enough to pass the selection threshold. Events with two or more  $b$ -tagged jets are assigned to either the two loose  $b$ -tags or two tight  $b$ -tags category, depending on the sum of the two highest  $b$ -ID discriminant values among the  $b$ -tagged jets. The operating point for the loose threshold has an identification efficiency of  $\approx 79\%$  for  $b$ -jets with a misidentification rate of  $\approx 11\%$  for light-flavor jets, while the point used to set the tight  $b$ -tag threshold has an efficiency of 50% for  $b$ -jets and a misidentification rate of 1.5% for light-flavor jets.

After applying these selection criteria, the expected event yields for the backgrounds and for a Higgs boson with  $M_H = 115$  GeV are compared to the observed number of events in Table I. Distributions of the dijet invariant mass, using the two jets of highest  $b$ -ID output (or highest  $p_T$  jets if fewer than two  $b$ -tagged jets are available), in  $W+2$ -jets and  $W+3$ -jets events are shown for the each  $b$ -tag category in each lepton channel in Figs 1 and 2. The data are well described by the predicted background. The contributions expected from a Higgs boson with  $M_H = 115$  GeV ( $H \rightarrow b\bar{b}$ ) and 130 GeV ( $H \rightarrow WW$ ) are also shown. The total signal contribution from  $H \rightarrow b\bar{b}$  decay channels decreases as  $M_H$  increases, while the total signal contribution from  $H \rightarrow WW$  decay channels has the opposite trend. At  $M_H \approx 130$  GeV and higher, the  $H \rightarrow WW$  decay channels significantly contribute to the search sensitivity.

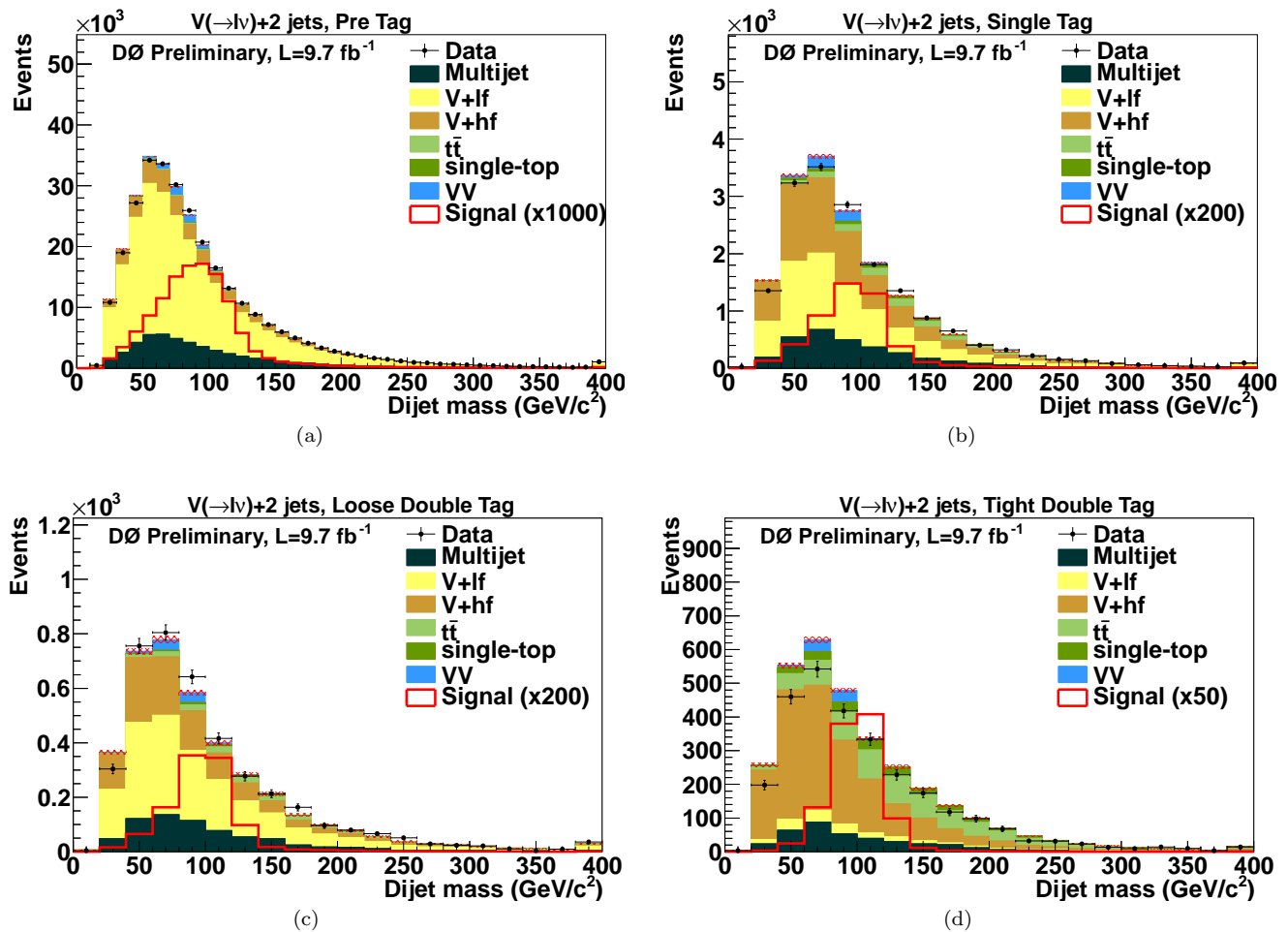


FIG. 1: Dijet mass distribution for all Run II electron and muon channel 2-jet events (a) before  $b$ -tagging, (b) with one tight  $b$ -tag, (c) with two loose  $b$ -tags, (d) with two tight  $b$ -tags. Events are scaled by a factor of 1000 before  $b$ -tagging; one  $b$ -tag events are scaled by a factor of 200; two loose  $b$ -tags by 200; two tight  $b$ -tags by 50. The signal shown is for a Higgs mass of 115 GeV.

To further separate signal and background we apply a Boosted Decision Tree (BDT) to the selected events. A BDT is created for each channel using the kinematic variables described in Table II. When selecting input variables we ensure that each is well-modeled and displays good separation between signal and one or more backgrounds. We train a separate BDT for each Higgs mass considered, with  $M_H$  varying between 100–150 GeV in 5 GeV steps, for each of the 48 independent channels for Run II data epochs. All channels are considered simultaneously when performing

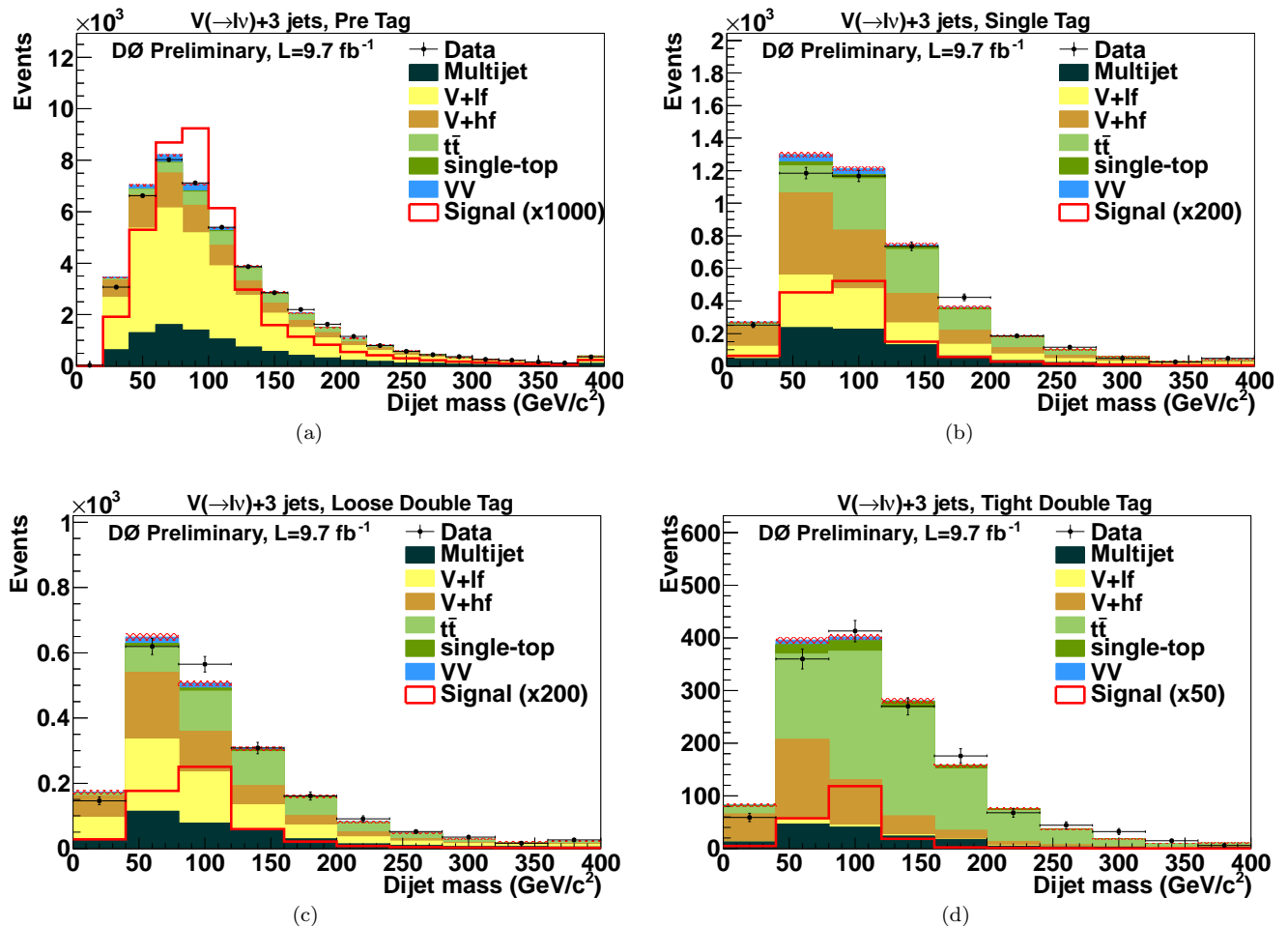


FIG. 2: Dijet mass distribution, using the highest  $b$ -ID output jets (or highest  $p_T$  jets if less than two  $b$ -tagged jets are available) for all Run II electron and muon channel 3-jet events (a) before  $b$ -tagging, (b) with one tight  $b$ -tag, (c) with two loose  $b$ -tags, (d) with two tight  $b$ -tags. Events are scaled by a factor of 1000 before  $b$ -tagging; one  $b$ -tag events are scaled by a factor of 200; two loose  $b$ -tags by 200; two tight  $b$ -tags by 50. The signal shown is for a Higgs mass of 115 GeV.

our limit calculations. Figure 3 shows the BDT output distributions for all 2-jet event channels.

## VII. SYSTEMATIC UNCERTAINTIES

The systematic uncertainties that affect the signal and backgrounds can be categorized by the nature of their source, i.e., theoretical (e.g., uncertainty on a cross section), modeling (e.g., re-weighting of ALPGEN samples), or experimental (e.g., uncertainty on integrated luminosity). Some of these uncertainties affect only the normalization of the signal or backgrounds, while others also affect the differential distribution of the BDT output.

Theoretical uncertainties include uncertainties on the  $t\bar{t}$  and single top-quark production cross sections (7% each [24, 25]), an uncertainty on the diboson production cross section (6% [26]), an uncertainty on  $W/Z$ +light-flavor production (6%), and an uncertainty on  $W$ +heavy-flavor production (20%, estimated from MCFM). These uncertainties affect only the normalization of these backgrounds.

Uncertainties from modeling that affect the distribution of the BDT output include uncertainties on trigger efficiency as derived from data (3–5%), lepton identification and reconstruction efficiency (5–6%), re-weighting of ALPGEN MC samples (2%), the MLM matching applied to  $W/Z$ +light-jet events ( $\approx 0.5\%$ ), and the systematic uncertainties associated with choice of renormalization and factorization scales in ALPGEN as well as the uncertainty on the strong coupling constant (2%). Uncertainties on the ALPGEN renormalization and factorization scales are evaluated by adjusting the nominal scale for each, simultaneously, by a factor of 0.5 and 2.0.

Experimental uncertainties that affect only the normalization of the expected signal and simulated backgrounds

TABLE I: Summary of event yields for the  $\ell + 2$  or 3 jets +  $\cancel{E}_T$  final states in Run II data. Events in data are compared with the expected number of events in the  $W+2$ - and  $W+3$ -jets samples, in simulated samples of diboson (including  $WW$ ,  $WZ$ , and  $ZZ$  processes),  $W/Z+b\bar{b}$  or  $c\bar{c}$ ,  $W/Z$ +light-quark jets, top quark (“ $t\bar{t}$ ” and “Single top”) production, and the data-derived multijet background. The  $WH \rightarrow \ell\nu b\bar{b}$  and  $ZH \rightarrow \ell b\bar{b} + \cancel{E}_T$  signals are shown for  $M_H = 115$  GeV; all other signals are  $M_H = 130$  GeV. Uncertainties include only the contribution from statistics.

	$W(\ell+\cancel{E}_T) + 2$ jets			
	pre- $b$ -tagging	1 tight $b$ -tag	2 loose $b$ -tags	2 tight $b$ -tags
$WH \rightarrow \ell\nu b\bar{b}$	54.66±0.10	16.97±0.06	3.94±0.03	18.54±0.06
$ZH \rightarrow \ell b\bar{b} + \cancel{E}_T$	7.07±0.02	2.23±0.01	0.52±0.01	2.15±0.01
$gg \rightarrow H \rightarrow WW \rightarrow \ell\nu jj$	31.22±0.17	2.45±0.04	0.39±0.02	0.17±0.01
$gg \rightarrow H \rightarrow ZZ \rightarrow \ell\ell jj$	0.74±0.01	0.08±< 0.01	0.02±< 0.01	0.03±< 0.01
$VV \rightarrow H \rightarrow WW \rightarrow \ell\nu jj$	4.64±0.03	0.29±0.01	0.07±< 0.01	0.02±< 0.01
$VH \rightarrow VWW \rightarrow \ell\nu + 4j$	17.69±0.10	1.65±0.03	0.31±0.01	0.13±0.01
Diboson	5858.9±6.6	548.9±1.9	103.0±0.8	88.3±0.5
$W + b\bar{b}$	8511.8±8.4	2881.4±4.8	385.3±2.1	1211.9±3.4
$Z + b\bar{b}$	877.8±1.1	301.7±0.6	38.5±0.2	107.2±0.4
$W + c\bar{c}$	20483±19	2596.0±6.8	565.1±3.3	325.4±2.4
$Z + c\bar{c}$	1959.7±2.3	250.3±0.8	53.3±0.4	30.7±0.3
$t\bar{t}$	2518.7±2.4	871.6±1.5	169.3±0.7	654.5±1.1
Single top	1116.5±1.2	451.9±0.8	56.7±0.3	205.6±0.4
Multijet	49249±92	3126.6±23.7	694.1±11.0	372.7±7.3
$W + (u, d, s)$ -jets	189474±98	5977.8±15.9	1710.5±8.1	163.4±2.3
$Z + (u, d, s)$ -jets	14827±15	393.1±2.2	119.6±1.1	9.4±0.3
Total expectation	294876±136	17399±14	3895.5±121.3	3169.0±8.8
Observed Events	295722	17231	4006	2790

	$W(\ell+\cancel{E}_T) + 3$ jets			
	pre- $b$ -tagging	1 tight $b$ -tag	2 loose $b$ -tags	2 tight $b$ -tags
$WH \rightarrow \ell\nu b\bar{b}$	10.76±0.04	3.09±0.02	1.30±0.02	3.05±0.02
$ZH \rightarrow \ell b\bar{b} + \cancel{E}_T$	1.91±0.01	0.55±0.01	0.25±< 0.01	0.50±0.01
$gg \rightarrow H \rightarrow WW \rightarrow \ell\nu jj$	7.89±0.09	0.70±0.02	0.28±0.02	0.09±0.01
$gg \rightarrow H \rightarrow ZZ \rightarrow \ell\ell jj$	0.23±< 0.01	0.03±< 0.01	0.01±< 0.01	0.01±< 0.01
$VV \rightarrow H \rightarrow WW \rightarrow \ell\nu jj$	4.56±0.03	0.40±0.01	0.17±0.01	0.03±< 0.01
$VH \rightarrow VWW \rightarrow \ell\nu + 4j$	10.21±0.07	1.19±0.02	0.46±0.02	0.13±0.01
Diboson	1141.5±2.9	113.5±0.9	49.1±0.6	19.4±0.3
$W + b\bar{b}$	1750.0±3.5	558.9±1.9	168.1±1.2	234.6±1.3
$Z + b\bar{b}$	230.0±0.6	77.1±0.3	22.4±0.2	32.1±0.2
$W + c\bar{c}$	4654.9±9.1	636.1±3.3	290.6±2.3	82.5±1.1
$Z + c\bar{c}$	532.9±1.2	74.5±0.4	36.2±0.3	10.5±0.2
$t\bar{t}$	3385.1±3.5	1017.2±1.9	429.0±1.3	854.9±1.6
Single top	293.0±0.7	97.0±0.4	33.1±0.2	67.6±0.3
Multijet	8905.1±40.8	770.8±11.7	340.1±7.5	149.0±4.2
$W + (u, d, s)$ -jets	22505±29	867.2±5.5	568.3±4.5	17.3±0.7
$Z + (u, d, s)$ -jets	2437.4±5.7	88.2±1.0	56.3±0.8	1.4±0.1
Total expectation	45835±52	4300.4±9.3	1993.3±42.7	1469.3±4.9
Observed Events	45262	4184	2019	1443

arise from the uncertainty on integrated luminosity (6.1%) [36]. Those that affect the BDT distribution include jet taggability (3%),  $b$ -tagging efficiency (2.5–3% per heavy quark-jet), the light-quark jet misidentification rate (10%), jet identification efficiency (5%); jet-energy calibration and resolution (varying between 15% and 30%, depending on the process and channel). The multijet background model has a contribution from the statistical uncertainty of data after tagging (10–20%), which also covers the uncertainty in the flavor dependence of  $f_{T|L}$ . We do not apply an additional uncertainty on the  $W$ +light jets normalization after  $b$ -tagging aside from that included in the systematic sources already mentioned.

## VIII. RESULTS

We observe no significant excess relative to the SM expectation and proceed to set upper limits on  $\sigma(H)$  using BDT discriminants for the different channels. All bins of the BDT distribution are examined to assure sufficient Monte Carlo (MC) statistics to protect against bins with zero background expectation. Those bins that do not have sufficient statistics are combined with adjacent bins until the signal and background expectations are large enough that the dominant uncertainty on the predictions is not due to the MC statistics. As described above, each channel is analyzed independently and the limits are then combined. We calculate all limits at 95% C.L. using the modified Frequentist  $CL_s$  approach with a Poisson log-likelihood ratio as the test statistic [37–39]. We treat systematic uncertainties as “nuisance parameters” constrained by their priors, and the best fits of these parameters are determined at each value of  $M_H$  by maximizing the likelihood. We remove the  $W/Z$ +jets normalization obtained from the  $M_W^T$  and muon  $p_T/\cancel{E}_T$  distributions and allow the components to vary by the aforementioned 6% and 20% uncertainties on

TABLE II: Table of BDT discriminant input variables.

Variable	Definition
$b$ -ID output	summed $b$ -tagging algorithm outputs for leading and sub-leading jets
$m_{bb}$	invariant mass formed by the pair of jets with the highest $b$ -tagging algorithm output values
$WH$ asymmetry	Mass asymmetry between $W$ and $H$ candidates: $(m_W - m_{bb})/(m_W + m_{bb})$
$H$ decay product velocity	$-\log\left(1 - \sqrt{1 - 4\sqrt{(m_1 + m_2)/m}}\right)$ where $m_1, m_2$ , and $m$ are respectively the leading, sub-leading and di-jet invariant masses
$q^\ell \times \eta_\ell$	lepton charge times pseudorapidity
$\Delta\eta_{max}(j, \ell)$	the maximum $\Delta\eta$ between any jet and the lepton
$\Sigma_{min}$	$\frac{\Delta R(j_1, j_2) \times p_T^{j, min}}{\sum p_T^j}$ , where $p_T^{j, min}$ corresponds to the smallest jet transverse momentum
$(\vec{p}_T^\ell + \vec{\cancel{E}}_T)/(p_T^\ell + \cancel{E}_T)$	vector sum of the lepton $p_T$ and $\cancel{E}_T$ over their scalar sum
Aplanarity	$3\lambda_3/2$ where $\lambda_3$ is the smallest eigenvalue of the normalized momentum tensor $S^{\alpha\beta} = \frac{\sum_i p_i^\alpha p_i^\beta}{\sum_i  p_i ^2}$ , where $\alpha, \beta = 1, 2, 3$ correspond to the $x, y, z$ momentum components and $i$ runs over the jets and lepton
$q^\ell \times \eta_{j1}$	lepton charge times the leading jet pseudorapidity
$m_{\ell\nu j2}$	invariant mass of lepton, neutrino and second leading jet
Centrality	$\frac{\sum_i p_T^j}{\sum_i  p_i }$ where $i$ runs over the jets and lepton
$p_T^{j2}$	second leading jet $p_T$

$W$ +light-flavor and  $W$ +heavy-flavor production. Independent fits are performed to the background-only and signal-plus-background hypotheses. All correlations are maintained among channels and between signal and background. Figure 4 shows the background-subtracted data along with the best-fit  $\pm 1\sigma$  systematic uncertainties, and the signal contribution for the Run II data set. The log-likelihood ratios for the background-only model and the signal-plus-background model as a function of  $M_H$  are shown in Fig. 5(a). The upper limit at 95% C.L. on the cross section for  $\sigma(p\bar{p} \rightarrow X + H) \times \mathcal{B}(H \rightarrow b\bar{b} \text{ or } WW)$  for  $M_H = 115$  GeV ( $M_H = 130$  GeV) is a factor of 3.96 (4.88) larger than the SM expectation and our expected sensitivity is 3.15 (6.11). The same study is performed for all other  $M_H$  values between 100 and 150 GeV. The corresponding observed and expected 95% C.L. limits relative to the SM expectation are given in Table III and in Fig. 5.

TABLE III: Observed and expected 95% C.L. upper limits on the ratio of  $\sigma(p\bar{p} \rightarrow X + H) \times \mathcal{B}(H \rightarrow b\bar{b} \text{ or } WW)$  to the SM expectation for each  $M_H$  value considered.

$M_H$ (GeV)	100	105	110	115	120	125	130	135	140	145	150
Expected Limit / $\sigma_{SM}$	2.19	2.45	2.70	3.15	3.88	4.81	6.11	8.22	11.73	16.36	18.04
Observed Limit / $\sigma_{SM}$	1.82	2.04	3.02	3.96	5.42	6.25	4.88	8.42	7.73	13.02	8.37

In conclusion, a search for standard model Higgs production in  $\ell + \cancel{E}_T + \text{jets}$  final states using three categories of  $b$ -tagged jets has been performed with  $9.7 \text{ fb}^{-1}$  of integrated luminosity from the D0 detector. The results are in agreement with the expected background, and we set upper limits on  $\sigma(p\bar{p} \rightarrow X + H) \times \mathcal{B}(H \rightarrow b\bar{b} \text{ or } WW)$  relative to the SM expectations  $\sigma(\text{SM})$  for masses of the Higgs boson between 100 and 150 GeV, as summarized in Table III and shown in Fig. 5. For  $M_H = 115$  GeV ( $M_H = 130$  GeV), the ratio of the observed 95% C.L. limit/(SM) is 3.96 (6.11) and the expected limit ratio is 3.15 (6.11).

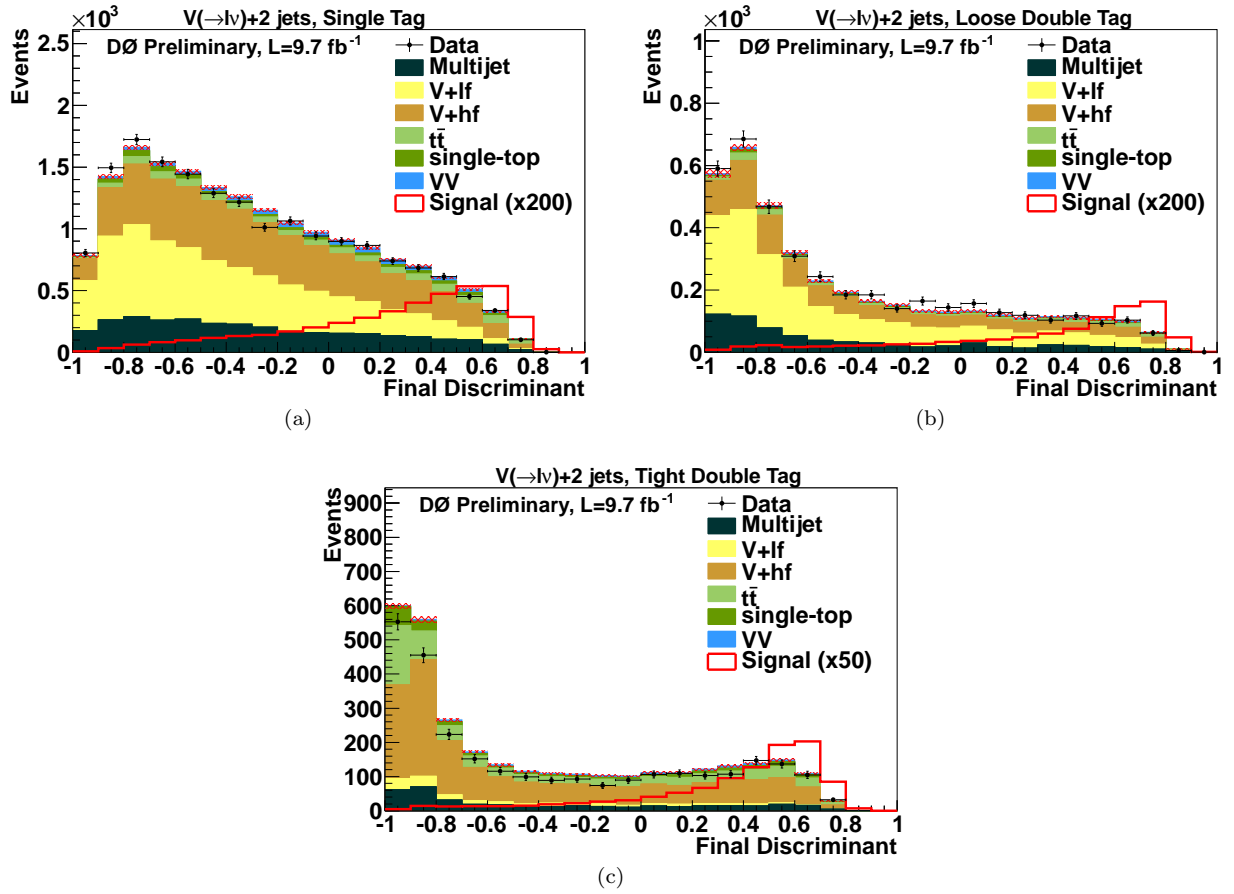


FIG. 3: Higgs signal multivariate discriminant output, for  $M_H = 115$  GeV, for Run II events with an electron or muon and two jets with (a) one tight  $b$ -tag, (b) two loose  $b$ -tags, and (c) two tight  $b$ -tags. Events are scaled by a factor of 1000 before  $b$ -tagging; one  $b$ -tag events are scaled by a factor of 200; two loose  $b$ -tags by 200; two tight  $b$ -tags by 50. The signal shown is for a Higgs mass of 115 GeV.

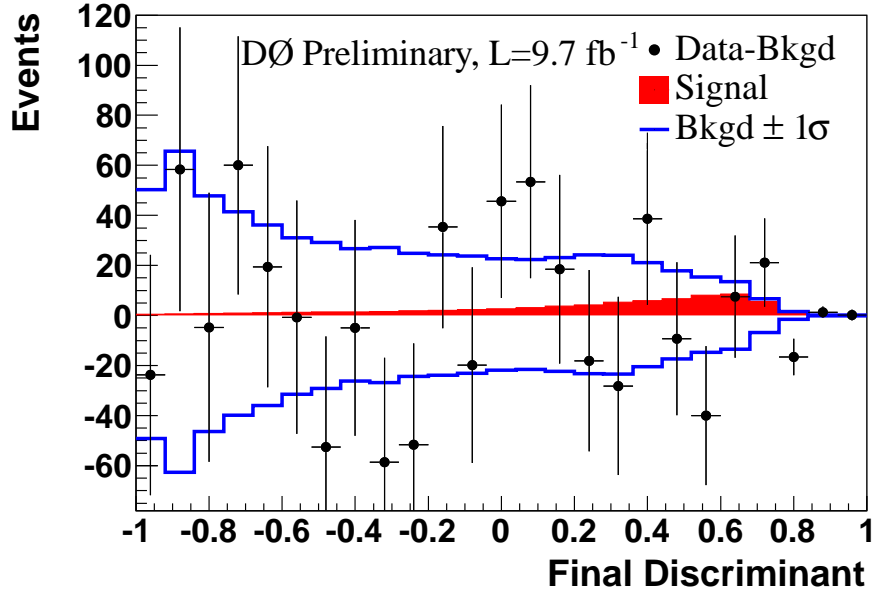
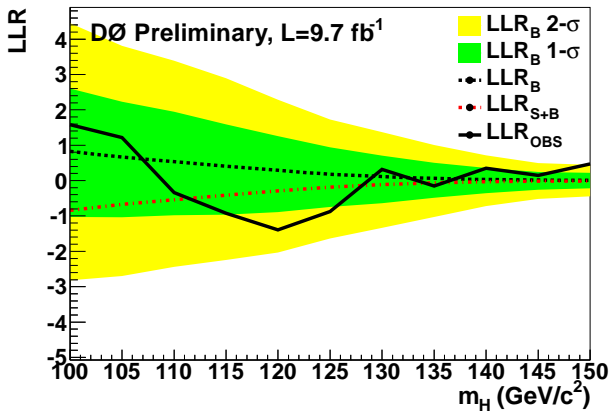
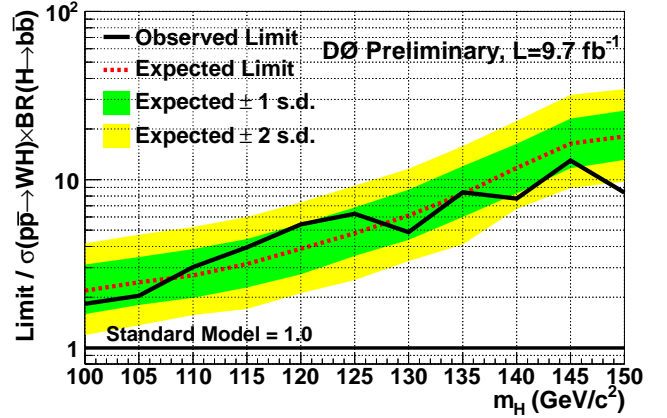


FIG. 4: Distribution in the output of the BDT discriminant for  $M_H = 115$  GeV for the difference between data and background expectation, combined for all channels (both  $e$  and  $\mu$ , and 2-jet and 3-jet, all  $b$ -tag categories), for the  $9.7 \text{ fb}^{-1}$  Run II dataset, shown with statistical uncertainties. The solid lines represent the total systematic uncertainty after constraining with data. The darker shaded region represents the SM Higgs signal expectation.



(a)



(b)

FIG. 5: Results obtained with the full Run II data set of  $9.7 \text{ fb}^{-1}$ . (a) Log-likelihood ratio for the background-only model ( $LLR_B$ , with  $1\sigma$  and  $2\sigma$  uncertainty bands), signal+background model ( $LLR_{S+B}$ ) and observation in data ( $LLR_{OBS}$ ) vs.  $M_H$  for the 2- and 3-jet events, with all  $b$ -tag categories combined. (b) The 95% C.L. cross section upper limit (and corresponding expected limit) on  $\sigma(p\bar{p} \rightarrow X + H) \times \mathcal{B}(H \rightarrow b\bar{b} \text{ or } WW)$  relative to the SM expectation vs.  $M_H$  for all channels combined.

## IX. ACKNOWLEDGEMENTS

We thank the staffs at Fermilab and collaborating institutions, and acknowledge support from the DOE and NSF (USA); CEA and CNRS/IN2P3 (France); FASI, Rosatom and RFBR (Russia); CNPq, FAPERJ, FAPESP and FUNDUNESP (Brazil); DAE and DST (India); Colciencias (Colombia); CONACyT (Mexico); KRF and KOSEF (Korea); CONICET and UBACyT (Argentina); FOM (The Netherlands); STFC and the Royal Society (United Kingdom); MSMT and GACR (Czech Republic); CRC Program and NSERC (Canada); BMBF and DFG (Germany); SFI (Ireland); The Swedish Research Council (Sweden); and CAS and CNSF (China).

- 
- [1] LEP Working Group for Higgs boson searches, R. Barate *et al.*, Phys. Lett. B **565**, 61 (2003).  
[2] Lep electroweak working group, <http://lepewwg.web.cern.ch/LEPEWWG/>.  
[3] TEVNP (Tevatron New Phenomena and Higgs Working Group), (2011), arXiv:1107.5518.  
[4] G. Aad *et al.*, (2012), arXiv:1202.1408.  
[5] S. Chatrchyan *et al.*, (2012), arXiv:1202.1488.  
[6] V. M. Abazov *et al.*, Phys. Rev. Lett. **94**, 091802 (2005).  
[7] V. Abazov *et al.*, Phys. Lett. B **663**, 26 (2008).  
[8] V. M. Abazov *et al.*, Phys. Rev. Lett. **102**, 051803 (2009).  
[9] V. M. Abazov *et al.*, Phys. Lett. B **698**, 6 (2011).  
[10] V. M. Abazov *et al.*, Phys. Rev. Lett. **106**, 171802 (2011).  
[11] V. M. Abazov *et al.*, Nucl. Instrum. Methods Phys. Res. A **565**, 463 (2006).  
[12] The pseudorapidity  $\eta = -\ln \left[ \tan \frac{\theta}{2} \right]$ , where  $\theta$  is the polar angle as measured from the beam axis;  $\phi$  is the azimuthal angle.  
The separation between two objects in  $\eta, \phi$  space is  $\Delta\mathcal{R} = \sqrt{(\Delta\eta)^2 + (\Delta\phi)^2}$ .  
[13] S. Abachi *et al.*, Nucl. Instrum. Methods Phys. Res. A **338**, 185 (1994).  
[14] R. Angstadt *et al.*, Nucl. Instrum. Methods Phys. Res. A **622**, 298 (2010).  
[15] M. Abolins *et al.*, Nucl. Instrum. Methods Phys. Res. A **584**, 75 (2008).  
[16] H. L. Lai *et al.*, Phys. Rev. D **55**, 1280 (1997).  
[17] J. Pumplin *et al.*, J. High Energy Phys. **07**, 012 (2002).  
[18] M. L. Mangano, M. Moretti, F. Piccinini, R. Pittau, and A. D. Polosa, J. High Energy Phys. **07**, 001 (2003).  
[19] T. Sjostrand, L. Lonnblad, S. Mrenna, and P. Z. Skands, (2003), hep-ph/0308153.  
[20] CompHEP, E. Boos *et al.*, Nucl. Instrum. Methods Phys. Res. A **534**, 250 (2004).  
[21] E. Boos *et al.*, Phys. Atom. Nucl. **69**, 1317 (2006).  
[22] R. Brun and F. Carminati, GEANT Detector Description and Simulation Tool, CERN Program Library Long Writup W5013, unpublished, 1993.  
[23] The Tevatron New Phenomena and Higgs Working Group, CDF Note 10474, 2012.  
[24] U. Langefeld, S. Moch, and P. Uwer, Phys. Rev. D **80**, 054009 (2009).  
[25] N. Kidonakis, Phys. Rev. D **74**, 114012 (2006).  
[26] J. Campbell and R. Ellis, Phys. Rev. D **60**, 113006 (1999).  
[27] J. Campbell, K. Ellis, and C. Williams, MCFM - Monte Carlo for FeMtobarn processes, <http://mcfm.fnal.gov/>.  
[28] R. Hamberg *et al.*, Nucl. Phys. B **359**, 343 (1991).  
[29] A. D. Martin, R. G. Roberts, W. J. Stirling, and R. S. Thorne, Phys. Lett. B **604**, 61 (2004).  
[30] J. Campbell, (2001), hep-ph/0105226.  
[31] V. M. Abazov *et al.*, Phys. Rev. Lett. **101**, 062001 (2008).  
[32] D0, V. M. Abazov *et al.*, Phys. Rev. Lett. **102**, 251801 (2009), 0903.4800.  
[33] G. C. Blazey *et al.*, (2000), hep-ex/0005012.  
[34] J. Alwall *et al.*, Eur. Phys. J. C **53**, 473 (2008).  
[35] V. M. Abazov *et al.*, Nucl. Instrum. Methods Phys. Res. A **620**, 490 (2010).  
[36] T. Andeen *et al.*, (2007), FERMILAB-TM-2365.  
[37] T. Junk, Nucl. Instrum. Methods Phys. Res. A **434**, 435 (1999).  
[38] A. L. Read, J. Phys. G **28**, 2693 (2002).  
[39] W. Fisher, (2007), FERMILAB-TM-2386-E.